Layer-by-Layer Nanoparticles with a pH-Sheddable Layer for *in Vivo* Targeting of Tumor Hypoxia

Zhiyong Poon, Dongsook Chang, Xiaoyong Zhao, and Paula T Hammond*

The Koch Institute for Integrative Cancer Research at MIT, Department of Chemical Engineering, Massachusetts Institute of Technology, Cambridge, Massachusetts 02139, United States

ABSTRACT Inspired by the simplicity and versatility of layer-by-layer (LbL) assembly, we applied multilayered polyelectrolyte assemblies on nanoparticles to create viable systemic delivery systems. Focusing on tumor-specific delivery, LbL nanoparticles that exhibit a pH-sensitive outer stealth layer are demonstrated to target and be retained in hypoxic tumor regions. The neutral layers shed in response to acidity to reveal a charged nanoparticle surface that is readily taken up by tumor cells. The first *in vivo* demonstration of this mechanism of targeting is presented, as well as an initial examination of the mechanism of uptake of the nanoparticles. We further demonstrate that this concept for tumor targeting is potentially valid for a broad range of cancers, with applicability for therapies that target hypoxic tumor tissue.

KEYWORDS: layer-by-layer · nanoparticles · drug delivery

Multilayered, multifunctional nanoparticles that are assembled *via* a layer-by-layer (LbL) deposition technique[1−4] are being explored as important new systems for systemic drug and gene delivery. A key design element that distinguishes these delivery vehicles from conventional systems[5−8] is the ability to use the assembled polymer layers to carry and control the release of therapeutics as well as to impart *in vivo* functionality.[9−11] LbL is a facile technique that is adaptable to a wide range of biologically relevant materials and therapeutics. Ideally, when the layer materials have been appropriately selected and the layer order is carefully designed, multifunctional LbL NPs can be rapidly fabricated in a built-to-order fashion,[10,12] making this delivery system an extremely attractive option for the scale-up of industrial applications.

Other studies have highlighted the viability of LbL-assembled nanoparticles for drug delivery[11−15] and have formed the basis for development of these systems in general. To the best of our knowledge, the primary emphasis thus far has been on the use of the LbL film as a non-erodible regulatory membrane for release of the core content, and there have been no attempts to build the capability to target tumors within the film architecture.[16−19] After long circulating nanoparticles accumulate passively in tumor interstitials, there is mounting evidence that the incorporation of targeting moieties improves nanoparticle uptake by cancer cells and prolongs their residence times in the tumor.[20−22] If the means to impart these capabilities can be applied to LbL-based particle systems, it would greatly impact their development toward clinical use. A frequent approach to gain tumor selectivity is by coating the surfaces of LbL particles with targeting ligands that are specific for cancer cells.[23,24] These biofunctionalization strategies are, however, restricted to gentler chemistries that are compliant with electrostatically assembled nanoparticles. Herein, we seek to demonstrate a pH-based strategy that takes advantage of the charged nature of multilayers to confer tumor specificity through the use of erodible nanofilms built within the LbL layers of nanoparticles.

We inhibit the nonspecific cellular uptake of positively charged LbL nanoparticles with a poly(ethylene glycol) (PEG) layer, which can be selectively removed by acidity generated in the hypoxic tumor microenvironment,[25,26] and show that this strategy for shielding and deshielding charges on LbL nanoparticles gives the capability to target tumors generically. Systems that utilize a tumor microenvironmental trigger, such as the presence of proteases,[27,28] or a reducing[29] or acidic environment[30−35] to affect drug delivery, are already in various phases of investigation. A pH-based strategy for targeting of tumors typically takes advantage of the lowered tumor pH to trigger disassembly of a carrier with subsequent drug release or to present cell targeting ligands that are hidden under physiological conditions.[36−38] These approaches have been shown to be therapeutically more advantageous when

* Address correspondence to hammond@mit.edu.

Received for review March 6, 2011 and accepted April 23, 2011.

Published online April 23, 2011
10.1021/nn200876f

compared to conventional pH-insensitive counterparts. Additionally, as hypoxia and subsequent acidosis are orchestrating forces for tumor cells to acquire resistance to chemotherapy and radiation,[39,40] this form of targeting also provides opportunities for therapies that sensitize hypoxic tumor cells to treatment.[41,42] Here we present the use of the native extratumoral pH in hypoxic tumors as a means of locally unveiling positively charged nanoparticle surfaces that are taken up by tumor cells *via* charge interactions.

RESULTS AND DISCUSSION

pH-Dependent Erosion of LbL Film. To demonstrate a concept for gaining tumor cell selectivity *via* the erosion of LbL layers, we utilize a trilayer architecture of poly-L-lysine (PLL) modified with iminobiotin, followed by the linker protein neutravidin and biotin end-functionalized poly(ethylene glycol) (PEG). This schematic illustration is shown in Figure 1A. The first, PLL layer improves cellular uptake of nanoparticles. The second, neutravidin (nav) layer bridges PLL and PEG *via* neutravidin−iminobiotin bonds.[43] Iminobiotin and neutravidin are modified versions of biotin and avidin, respectively, and the iminobiotin−neutravidin interaction is a pH-dependent nonchemical bond akin to the biotin−avidin bond.[44] Iminobiotin−neutravidin bonds are stable at pH 8−12 but are easily decomposed at pH 4−6 as a result of the lower affinity of the protonated iminobiotin to neutravidin (Figure 1B). Lastly, the terminal, PEG layer is a commonly used antifouling polymer that would enable the layered nanoparticles to avoid rapid reticuloendothelial system (RES) clearance,[45] allowing their accumulation in tumor interstitials due to the enhanced permeation and retention effect[46] (EPR). When these nanoparticles accumulate in the acidic tumor environment, we hypothesized that they would gradually lose their PEG shells as the iminobiotin−neutravidin interactions decreased, allowing the exposed PLL layer to facilitate cellular uptake, thus shifting the biodistribution of the layered nanoparticles to favor tumor retention.

Cellular Uptake of PLL-Coated Nanoparticles. As this strategy for gaining tumor selectivity relies on exposing a positively charged PLL layer to cancer cells for uptake, it is first important to examine the cellular uptake of positively charged PLL-coated nanoparticles to understand the mechanism for charge-mediated uptake. Flow cytometry measurements in Figure 2A show that even a single terminal layer of PLL was able to bring about notably increased levels (at least 5× increase) of nanoparticle uptake with HeLa cells. Cellular internalization of PLL-coated fluorescent latex beads was confirmed with confocal microscopy (Figure 2C(ii)). In comparison to uncoated fluorescent latex beads coincubated with cells using an estimated amount of PLL equivalent to one layer (HPLC estimates based on mass

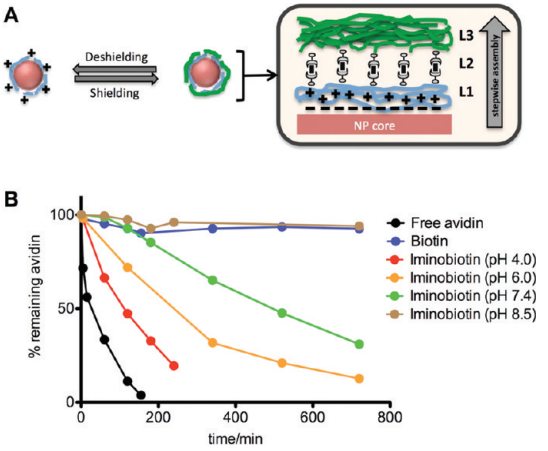

Figure 1. (A) Schematic illustration of the design and concept for achieving tumor specificity with layer-by-layer nanoparticles. This design takes advantage of a lowered pH in hypoxic tissues to deshield the terminal, poly(ethylene glycol) layer, exposing the underlying positively charged poly-L-lysine layer for cell targeting. L1: PLL modified with iminobiotin; L2: neutravidin; L3: biotin end-functionalized PEG. (B) Rate of loss of avidin−FITC from iminobiotin conjugated to polyethyleneimine (500 kDa). The pH dependence of the iminobiotin−avidin bond used to predict behavior of the iminobiotin−neutravidin bond. This bond is stable above pH 8.0 but gradually dissociates at pH 7.4. In acidic conditions (pH < 6), the bond rapidly breaks down.

conservation calculations), as well as a second control with 10 times this estimated amount, PLL-coated latex beads induced a significantly greater amount (∼4−10× increase) of cell uptake (Figure 2A). When the topmost layer of the LbL film was dextran sulfate (DXS), yielding a negatively charged surface, cellular uptake decreased. This alternating trend of cellular uptake for positively (PLL) or negatively (DXS) charged terminal layers was consistent even as the LbL films were built thicker (Figure 2B). The procedure for LbL deposition of PLL/DXS on sulfonated latex beads is given in the experimental section, and Figure S1 (see Supporting Information) shows the average hydrodynamic diameter and zeta potential of these particles during LbL film construction.

The mechanism of cell uptake of positively charged LbL nanoparticles was studied with confocal microscopy and flow cytometry analysis (Figure 2C and D). Images from each individual fluorescence channel for Figure 2C are shown in Figure S2 (see Supporting Information). From confocal analysis (Figure 2C), incubation times between 30 min and 2 h were found to be necessary for inducing nanoparticle uptake by HeLa cells. Once taken up by HeLa cells, the layered nanoparticles were observed to internalize with transferrin, a well-studied molecule that undergoes clathrin-mediated endocytosis. Co-localization of transferrin and nanoparticle occurred downstream of the internalization pathway (2 h) but not at early times (30 min), indicating that the nanoparticles are taken into the cell in a manner that is separate from and slower than

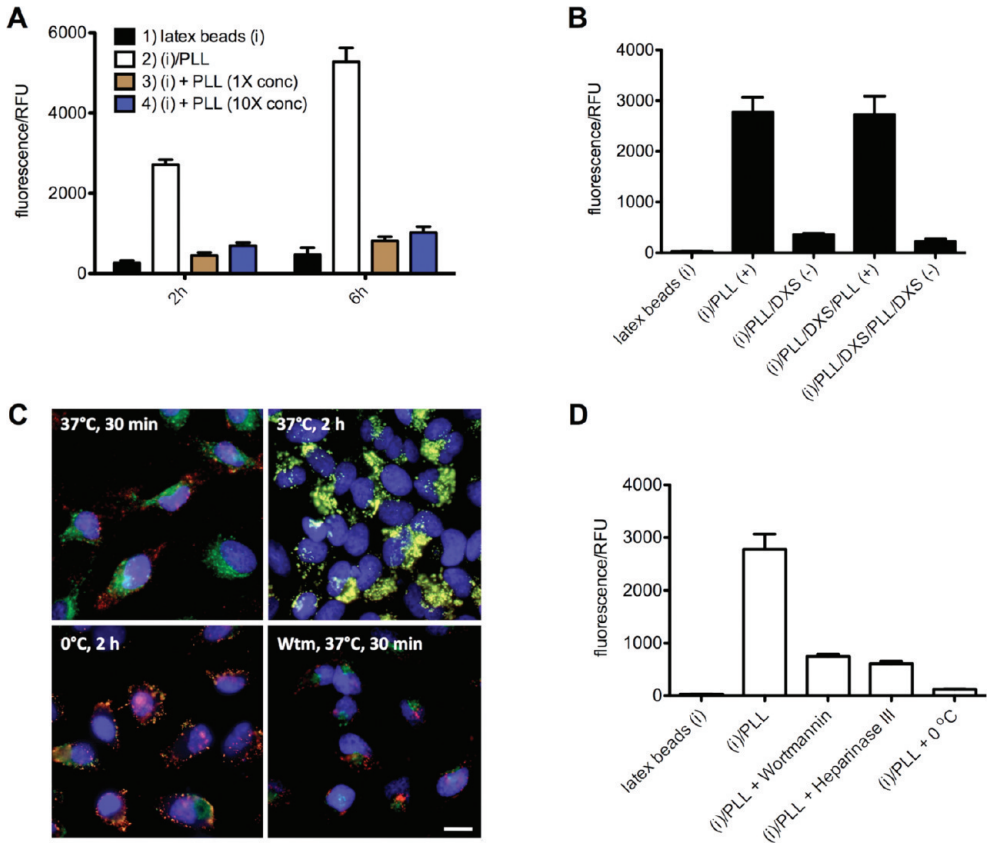

Figure 2. (A) Flow cytometry analysis of HeLa cells incubated with (1) fluorescent sulfonated latex beads (i), (2) (i) with a PLL layer, (3/4) (i) co-incubated with PLL at different concentrations. In comparison to uncoated fluorescent latex beads co-incubated with cells using an estimated amount of PLL equivalent to one layer (HPLC estimates based on mass conservation calculations), as well as a second control with 10 times this estimated amount, PLL-coated latex beads induced a significantly greater amount (~4–10× increase) of cell uptake. (B) The uptake of LbL nanoparticles can be enhanced or diminished by the terminal layer charge. LbL nanoparticles with positive zeta potentials (PLL terminated) are taken up by cells more readily than nanoparticles with negative zeta potentials (DXS terminated). This trend is consistent as the film thickness increases. (C) Confocal microscopy analysis of HeLa cells given different PLL-coated LbL nanoparticles under different conditions described in the image (Wtm: wortmannin treatment, 0 °C indicates treatment of cells on ice). The cell fluorescence measured by flow cytometry was due to internalized nanoparticles. Internalized particles co-localized with transferrin downstream of the internalization pathway but not at early times, indicating that the nanoparticles are taken into the cell in a manner that is separate from and slower than transferrin endocytosis. Co-localization of both signals downstream indicate similar means of trafficking past 2 h. Additional control experiments with cells treated on ice and wortmannin show that the uptake of these particles is energy driven. Confocal images from each fluorescent channel are shown in Figure S2 (see Supporting Information). Red = LbL nanoparticle; green = transferrin; blue = nuclei; yellow = co-localization of LbL nanoparticle and transferrin. Scale bar = 10 μm. (D) Flow cytometry analysis of HeLa cells under different conditions described in Figure 2C. Additionally, treatment of cells with heparinase III, an enzyme that breaks down the negatively charged heparan sulfate found bound on cell surfaces, also significantly reduced positively charged nanoparticle uptake, showing that interactions of positive nanoparticles with negatively charged heparan sulfate on the cell surface play an important role for uptake. All flow cytometry analyses represent fluorescence from the entire single-cell population (10 000 events) and are presented as mean ± sem. Analyses in C and D are taken at the 2 h time point.

transferrin endocytosis. Experiments with cells treated on ice (0 °C) and wortmannin,[47] an inhibitor of clathrin-mediated processes, indicate that the mechanism of uptake for positively charged nanoparticles is energy driven. Quantitative results for these experiments were measured with flow cytometry analysis and are given in Figure 2D. Additionally, treatment of cells with heparinase III,[48] an enzyme that breaks down the negatively charged heparan sulfate found bound on cell surfaces, also significantly reduced positively charged nanoparticle uptake, showing that interactions of positive nanoparticles with negatively charged heparan sulfate on the cell surface play an important role for uptake (Figure 2D). Finally, the cytotoxicity of these positively charged LbL nanoparticles was found to be negligible when tested with a 3-(4,5-Dimethylthiazol-2-yl)-2,5-diphenyltetrazolium bromide (MTT) assay with HeLa cells (Figure S3, see Supporting Information). Polypeptides containing a high percentage of cationic amino acids, such as PLL, are used routinely to facilitate cellular uptake of a variety of biopolymers and small molecules.[49] The use of such polymers to significantly enhance cellular uptake of nanoparticles *via* their LbL deposition provides a convenient approach for LbL-based nanoparticles to gain cellular entry into well-studied pathways for the delivery of therapeutics.

LbL Nanoparticle Assembly and *in Vitro* Examination. After verifying that the charge shielding of PLL-coated LbL nanoparticles makes a significant difference in their cellular uptake, we sought to evaluate if the use of the trilayer architecture depicted in Figure 1A would allow LbL nanoparticles to gain tumor selectivity after their systemic injection. Assembly of the trilayers was carried out with carboxyl-functionalized near-infrared quantum dots (QD, em: 705 nm) as the charged core material that would allow building of polymer films and tracking of the particles *in vivo*. Before depositing the PLL layer, the side-chain primary amines on PLL were modified with iminobiotin (~20% of available side groups; PLLib) using N-hydroxysuccinimide (NHS) chemistry. Neutravidin and mPEG-biotin (~20 KDa) were subsequently layered onto the nanoparticle in a stepwise fashion (see Materials and Methods for full details). The deposition of each layer was followed by dynamic light scattering and zeta potential measurements (Table 1). Addition of the trilayer architecture (PLLib/nav/PEG) increased the hydrodynamic diameter of the original particles from ~20 nm to ~80 nm, with most of the increase attributed to the terminal, PEG layer. The zeta potential of the nanoparticle shifted from ~ −25 mV to ~ +30 mV with the deposition of PLLib and, finally, to ~0 mV when terminated with PEG. An SEM image of the QD/PLLib/nav/PEG particles is shown in Figure 3A. These particles are generally spherical and uniform in size after the LbL coating process.

To confirm that cellular uptake of the LbL particles can be restored after deshielding the terminal layer of PEG, we incubated different cancer cells with LbL nanoparticles subjected to pretreatments at pH 7.4 and 5.5 for 4 h. After acidic treatment (pH 5.5) QD/PLLib/nav/PEG particles decreased in average size and increased in charge (Table 1), indicating removal of the charge-shielding terminal, PEG layer (zeta potential shifted from ~0 mV to ~25 mV), while LbL particles incubated at pH 7.4 remained the same in size and charge. Deshielding the external PEG layer restored cellular uptake (Figure 3B); compared to LbL particles incubated at pH 7.4, those that were deshielded (pH 5.5 treatment) caused a greater amount of uptake in all tested cancer cell lines, suggesting that this strategy could be used as a generic way of targeting tumors, as an acidic microenvironment is a hallmark of all tumors.[25]

Targeting of Tumors *In Vivo*. Next, the utility of this tumor targeting strategy was tested *in vivo* with subcutaneous tumor models. Control nanoparticles were constructed by substituting iminobiotin (PLLib) for biotin (PLLb), which does not have a pH-dependent bond with neutravidin. The resulting particles (QD/PLLib/nav/PEG and QD/PLLb/nav/PEG) are less than 100 nm in size and have a near neutral zeta potential (Table 1). Their sub-100 nm sizes would facilitate their diffusion within the tumor tissue to more readily encounter hypoxic pockets. After systemic intravenous injection of the nanoparticles into mice, the blood concentrations of the nanoparticles decreased in a two-phase manner (Figure 4A). The significantly longer circulation profiles of the administered LbL particles compared to free QD due to the presence of the PEG nanolayer indicate a certain level of nanofilm stability while in systemic circulation. Initially, both QD/PLLib/nav/PEG and QD/PLLb/nav/PEG were observed to have a relatively similar circulation profile, with more than 25% of the particles still in the blood by 6 h; however, the blood level of QD/PLLib/nav/PEG was detected to be significantly lower than QD/PLLb/nav/PEG after 12 h. Blood concentrations of QD/PLLib/nav/PEG and QD/PLLb/nav/PEG had dropped to 1% and 14%, respectively, of the original amount by 24 h. The faster elimination of QD/PLLib/nav/PEG is likely due to the gradual removal of the terminal PEG layer while at physiological pH, as the iminobiotin−neutravidin bond is most stable above pH 8.0. This is supported by examinations of the iminobiotin−avidin bond (Figure 1B), which show a slow degradation of the bond at pH 7.4. The resulting exposure of the PLL layer leads to rapid elimination of the particles, presumably by processes of opsonization of the complement system.[50]

We monitored the accumulation of the particles in subcutaneously induced MDA-MB-435 (Figure 4B) and KB (Figure S4, see Supporting Information) tumors with intravital fluorescence imaging over a period of 48 h. For both tumor models (n = 3), accumulation of particles within the tumor reached a peak at the 8 h time point and steadily decreased thereafter, as particle elimination from the blood reservoir diminishes the effect of EPR-based tumor targeting.[51] The mechanisms of EPR[46,51,52] are not expected to discriminate between the two sets of nanoparticles, which have similar sizes, charges, surface properties, and blood circulation (in the initial period after injection), and equal levels of accumulation were observed in both tumor models at the 8 h point (Figure 4C, two-tailed

TABLE 1. Average Hydrodynamic Diameter and Zeta Potentials of LbL NPs[a]

LbL nanoparticle	effective diameter (nm)	PDI	zeta potential (mV)
QD	20 ± 5	1.09	−26 ± 4
QD/PLL	24 ± 6	1.21	+30 ± 5
QD/PLLib	24 ± 8	1.23	+33 ± 2
QD/PLLib/nav/PEG (pH 7.4)	76 ± 7	1.25	+1.3 ± 3
QD/PLLib/nav/PEG (pH 5.5)	38 ± 11	1.21	+25 ± 7
QD/PLLb/nav/PEG	82 ± 8	1.23	+0.7 ± 2

[a] QD = quantum dot; PLL= poly-L-lysine; PLLib = PLL functionalized with iminobiotin; PLLb = PLL functionalized with biotin; nav = neutravidin; PEG = biotin end-functionalized poly(ethylene glycol). The values shown are in mean ± SEM, where n = 10. The raw data for the number average diameters of QD, QD/PLLib, and QD/PLLib/nav/PEG are shown in Figure S1C.

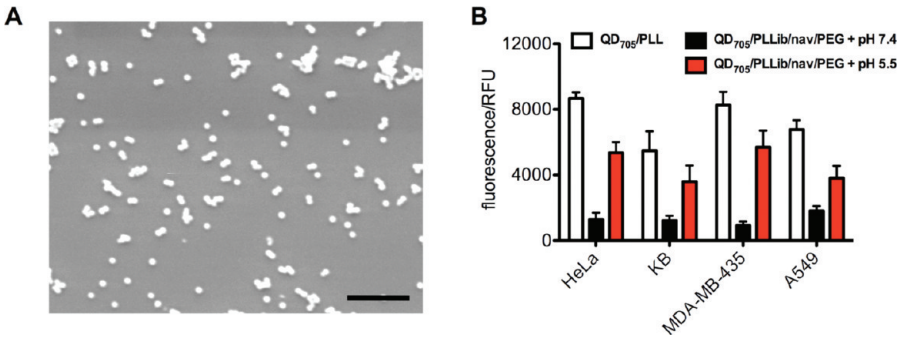

Figure 3. (A) SEM image of QD/PLLib/nav/PEG particles. These particles are generally spherical and uniform in size after the LbL coating process. Scale bar = 1 μm. (B) Cellular uptake of QD/PLLib/nav/PEG particles across a panel of cancer cell lines is restored after acidic pretreatment (pH 5.5 for 4 h), suggesting the potential to target a broad range of cancers with hypoxic microenvironments, as the LbL particles lose their PEG shells in the lowered pH environments of hypoxic tissue.

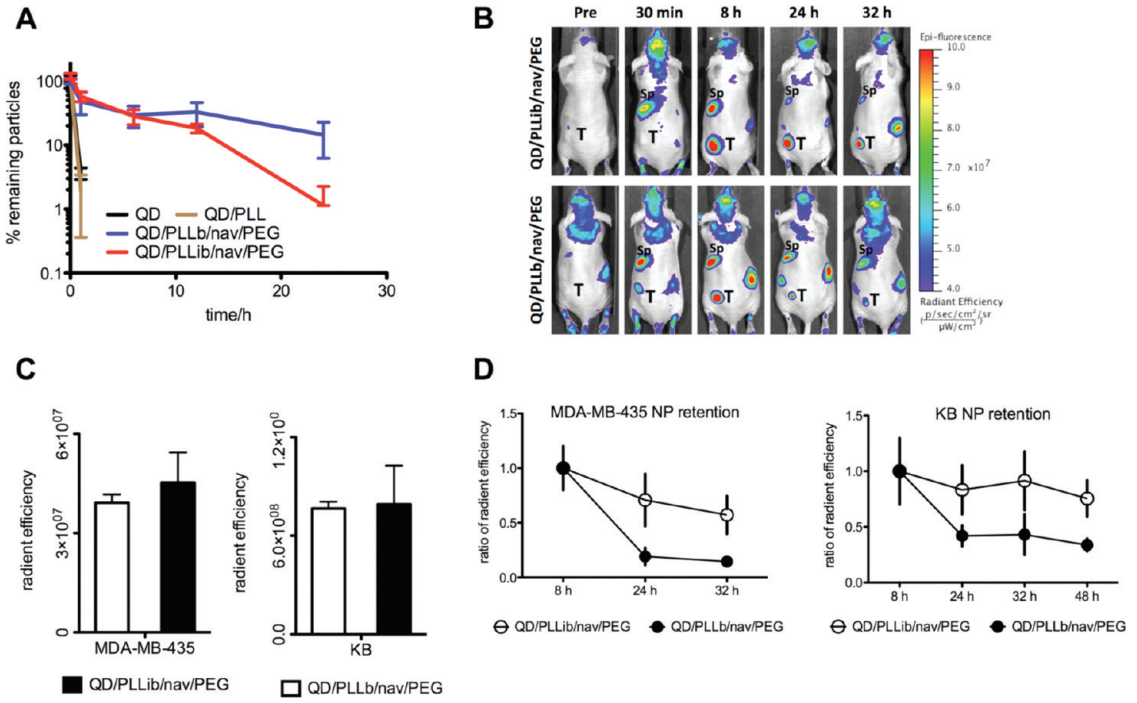

Figure 4. (A) Log−linear blood circulation profiles of QD, QD/PLL, QD/PLLib/nav/PEG, and QD/PLLb/nav/PEG. Changing the surface properties of QDs with LbL improves nanoparticle circulation. QD/PLLib/nav/PEG and QD/PLLb/nav/PEG have similar profiles up to 12 h post-administration. QD/PLLib/nav/PEG clears faster after 12 h. (B) Dorsal scans of representative mice showing the accumulation and clearance of LbL nanoparticles in MDA-MB-435 tumors (left hind flank). T = tumor; Sp = spleen. Similar images of mice with KB xenografts are shown in Figure S4A (see Supporting Information). (C) LbL nanoparticle accumulation levels in tumors at 8 h. There was no statistical difference between fluorescence from both particle types for each tumor model (95%; CI $P_{KB} = 0.92$, $P_{MDA\text{-}MD\text{-}435} = 0.56$). (D) Rate of clearance of nanoparticles from tumors relative to the 8 h time point. QD/PLLib/nav/PEG is cleared slower, demonstrating the deshielding of PEG and subsequent tumor cell targeting. The absolute levels of nanoparticle fluorescence are given in Figure S4C (see Supporting Information).

Student's *t* test shows no significant difference 95%; CI $P_{KB} = 0.92$, $P_{MDA\text{-}MD\text{-}435} = 0.56$); this is evidence of the dominance of the EPR-based targeting during this initial period.

After passing through vascular borders and accumulating within the tumor interstitials, LbL particles that may be deshielded by acidity do so in hypoxic regions, exposing the PLL layer for cellular uptake; therefore, for the 8 to 48 h period, the clearance of QD/PLLib/nav/PEG from tumors was much slower compared to QD/PLLb/nav/PEG, which are internalized by cells less readily and are slowly eliminated by the lymphatic system, as observed in the later time points for Figure 4B. Figure 4D shows the rate of nanoparticle clearance from both tumor models relative to the 8 h time point (the absolute values are given in Figures S4B and S4C, see Supporting Information). The stronger retention of QD/PLLib/nav/PEG demonstrates the

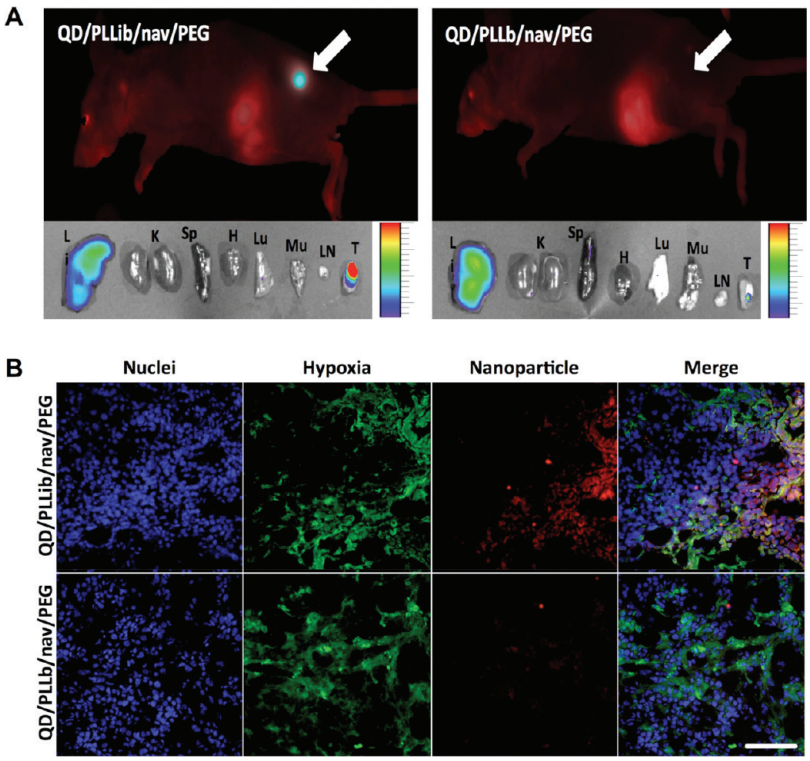

Figure 5. (A) Spectrally unmixed lateral scan of representative MDA-MB-435 mice model and biodistribution of nanoparticles in organs 48 h after administration. QD/PLLib/nav/PEG nanoparticle fluorescence was still present in tumors at 48 h, which suggests significant nanoparticle uptake by tumor cells. Red = tissue and food autofluorescence; teal = nanoparticle fluorescence. Li = liver; K = kidney; Sp = spleen; H = heart; Lu = lungs; Mu = muscle; LN = lymph nodes; T = tumor. Image is spectrally unmixed to separate the nanoparticle fluorescence from tissue autofluorescence. (B) Tumor sections (20×) from mice given QD/PLLib/nav/PEG or QD/PLL/nav/PEG. In tumors given QD/PLLib/nav/PEG treatments, a co-localization between nanoparticle and HIF-1α positive regions was found. Nanoparticle presence was not significant in tumors given QD/PLL/nav/PEG. Red = LbL nanoparticle; green = hypoxia; blue = nuclei. Scale bar = 50 μm.

deshielding of LbL particles to allow cellular interaction with the underlying PLL layer for improved uptake. Dissociation of the iminobiotin–neutravidin bond in the acidic tumor microenvironment can happen fairly rapidly (~50% dissociation within 3–4 h, Figure 1B), permitting a significant portion of the accumulated QD/PLLib/PEG particles to be deshielded within the 8 h EPR targeting window. This effect is manifest thereafter, which translates to a greater degree of particle retention observed in the tumors. Figure 5A shows the left lateral scan of a representative mouse (MDA-MB-435 tumor model) at the 48 h time point and the biodistribution of particles in harvested tissue from these mice; both sets of data clearly indicate stronger and longer retention of QD/PLLib/nav/PEG in tumors. Finally, histological examinations of tumor sections reveal a high level of association between the QD/PLLib/nav/PEG signal and regions stained for hypoxia (Figures 5B and S5, see Supporting Information). In contrast, the QD/PLLb/nav/PEG signal is considerably weaker and is not present in hypoxic regions; these data provide further evidence that the deshielding mechanism of the pH-sensitive LbL particles is responsible for their persistence in tumors, particularly in regions of hypoxia; this observation provides exciting new opportunities for chemotherapy to solid tumors and delivery of antihypoxic cancer therapies using the LbL nanoparticle approach.

CONCLUSION

In summary, this study illustrates a promising approach for systemic tumor targeting using LbL nanoparticles. We demonstrate proof of principle that the electrostatic assembly nature of LbL allows the use of charge to aid or inhibit their cellular uptake and extend this idea to enable tumor targeting *in vivo* by incorporating a pH-responsive layer that exposes the underlying charged surface when localized in an acidic tumor microenvironment. As EPR-based targeting is transient, strategies to extend the persistence of accumulated particles have the potential to greatly impact nanoparticle therapy. The stronger persistence of QD/PLLib/PEG particles in two different tumor models highlights a key advantage of this system: as hypoxia is ubiquitous in tumors, this form of targeting with LbL nanoparticles could be potentially employed to broadly target all cancers, even those that do not express distinctive surface markers. Looking forward, alternative material systems to iminobiotin and neutravidin should

be explored that can exhibit extended stability at physiological pH. Additionally, a more comprehensive study of the distribution of the pH-targeted LbL particles as well as their target cell type within different tumor types is planned in future work, to gain a better understanding of the efficacy of the system in different tumor microenvironments. Finally, there is potential to combine these systems with a range of molecular cargos or imaging agents for therapeutic or imaging applications.

MATERIALS AND METHODS

Materials. All chemicals and biological material were purchased from Sigma-Aldrich or Invitrogen unless otherwise noted.

Mice. Female Nu/Nu mice (4–6 weeks old) were from Taconic. All *in vivo* experimentation was carried out under the supervision of the Division of Comparative Medicine (DCM), Massachusetts Institute of Technology, and in compliance with the Principles of Laboratory Animal Care of the National Institutes of Health. Cell lines were purchased from ATCC and were tested routinely for pathogens before use in animals *via* DCM.

Fabrication of Layer-by-Layer Nanoparticles. LbL nanoparticles with functional shells were prepared using a commonly used assembly technique for LbL on nanoparticles.[53] The negatively charged fluorescent cores used were either sulfonated polystyrene beads (LB) ($\sim 5 \times 10^{13}$ particles/mL; ex/em: 575 nm/610 nm; ~130 nm; −35 mV; Sigma-Aldrich) or carboxylated quantum dots (8 μM; em: 705 nm; ~20 nm; −25 mV; Invitrogen). Pol-L-lysine was functionalized to NHS-activated iminobiotin (Thermo Scientific) or NHS-activated biotin (Sigma Aldrich) on ~20% of the primary amine side groups (based on reaction feed ratio) under aqueous conditions and at a pH of 8.0. After reacting for 2 h at room temperature, the functionalized peptides were then dialyzed in a 5 kDa dialysis bag before use. For LbL assembly, nanoparticles were mixed with a saturating amount of layering material with continuous agitation. Mixing was carried out for 2 h, followed by particle purification with three centrifugation (30 000 rcf; 2 h) and resuspension (Millipore water, pH 7.4) cycles. Layering conditions are as follows: for aqueous polymer solutions (poly-L-lysine (15 kDa), dextran sulfate (15 kDa); Sigma Aldrich), a final concentration of ~500 μM for 2 h; for neutravidin (Thermo Scientific), a saturating ratio of 1 mg of neutravidin to 0.05 mol of nanoparticle for 2 h; for mPEG-biotin (20 kDa; Laysan Bio), 100 mg of mPEG-biotin in aqueous conditions for 2 h. A pH of 7.4 was used in all cases except for situations involving iminobiotin, where a pH of 8.0 was used instead. No salt was added in the process.

Characterization of Particles. All size and zeta potential measurements were made using a Zeta PALS (Brookhaven), and scanning electron microscopy was performed on particles spin-cast on silicon. Particle concentrations were estimated using standard calibration graphs made from unmodified particles. These graphs were linear in the range of concentrations used for all experiments. For *in vitro* experiments, the concentration of particles used was fixed for any one set of experiments and ranged from 1×10^8 to 1×10^{10} particles/mL. For *in vivo* experiments, the concentration of particles used was ~0.1 μM given in 0.1 mL injections.

Examination of Neutravidin–Iminobiotin Bond. The pH dependence of this bond was investigated by conjugating iminobiotin to high molecular weight polyethyleneimine (500 kDa) *via* NHS chemistry followed by suspending the polyethyleneimide and avidin-FITC (Sigma Aldrich) complex inside a 100 kDa Float-a-lyzer (Spectrum Laboratories) in buffer sinks at different pH conditions. The contents of the Float-a-lyzer were tested regularly for FITC fluorescence with a spectrofluorometer.

***In Vitro* Experimentation.** HeLa, MDA-MB-435, KB, and A549 cells were cultured with Alpha MEM (Invitrogen) supplemented with heat-inactivated bovine serum (10%; Invitrogen) and penicillin/streptomycin (1%). For flow cytometry measurements, cells were plated on 96-well plates at 70% confluence a day before use. Treated cells were trypsinized, washed, and resuspended in PBS before analysis. Transferrin-FITC, wortmannin, and heparinase III (Sigma-Aldrich) were used at concentrations of 100 nM, 200 nM, and 0.1 U/mL. All measurements were made with 10 000 events and at least in triplicate. For confocal microscopy analysis, cells were washed, fixed in 10% formalin, and permeabilized with 70% ethanol before staining. For analysis of hypoxia, HIF-1α and the appropriate FITC-labeled secondary antibody (Santa Cruz Biotechnology) were used. Images were captured using an Applied Precision DeltaVision confocal. A Cy5 filter was used to detect quantum dot (em: 705 nm) fluorescence.

***In Vivo* Experimentation.** Subcutaneous tumors were induced in either the left or right hind flank after injection of ~1–2 million cells (MDA-MB-435 or KB, $n = 3$ each) in 0.1 mL of media. Tumors were allowed to grow to ~100 mm^3 before experimentation. The concentration of particles administered was ~0.1 μM given in 0.1 mL injections *via* the tail vein. All nanoparticle solutions were filtered with a 0.2 μm filter before injection. LbL nanoparticle accumulation *in vivo* was tracked and quantified using intravital imaging (Caliper LifeSciences). The images showing QD_{705} fluorescence were captured using ex: 640 nm and em: 720 nm. Spectrally unmixed images were captured using a sequence of ex: 640 nm and em: 700 nm/720 nm/740 nm/760 nm for QD_{705}. For histology, tumors were frozen in OCT (−80 °C) and cut into 5 μm sections for analysis. Blood circulation analysis was performed by measuring the remaining QD signal from blood taken after injection (tail vein) with a spectrofluorometer.

Statistical Analysis. All data in figures and text are given as mean ± SEM. Flow cytometry measurements were made with $n = 10\,000$ events and performed in triplicate at the minimum.

Acknowledgment. We wish to thank our funding source for this research, the National Institutes of Health (NIH) NIBIB grant R01EB008082 and The MIT-Harvard Center of Cancer Nanotechnology Excellence grant 1U54CA151884. We also thank the Koch Institute for Integrative Cancer Research (MIT), the Institute for Soldier Nanotechnology (ISN), and the Department of Comparative Medicine (DCM) at MIT for assistance with animal experiments and for use of facilities.

Supporting Information Available: Figures S1 to S4. This material is available free of charge *via* the Internet at http://pubs.acs.org.

REFERENCES AND NOTES

1. Decher, G.; Eckle, M.; Schmitt, J.; Struth, B. Layer-by-Layer Assembled Multicomposite Films. *Curr. Opin. Colloid Interface Sci.* **1998**, *3*, 32–39.
2. Hammond, P. T. Form and Function in Multilayer Assembly: New Applications at the Nanoscale. *Adv. Mater. (Weinheim, Ger.)* **2004**, *16*, 1271–1293.
3. Lynn, D. M. Peeling Back the Layers: Controlled Erosion and Triggered Disassembly of Multilayered Polyelectrolyte Thin Films. *Adv. Mater. (Weinheim, Ger.)* **2007**, *19*, 4118–4130.
4. Boudou, T.; Crouzier, T.; Ren, K.; Blin, G.; Picart, C. Multiple Functionalities of Polyelectrolyte Multilayer Films: New Biomedical Applications. *Adv. Mater. (Weinheim, Ger.)* **2010**, *22*, 441–467.

5. Davis, M. E.; Chen, Z.; Shin, D. M. Nanoparticle Therapeutics: An Emerging Treatment Modality for Cancer. *Nat. Rev. Drug Discovery* **2008**, *7*, 771–782.
6. Duncan, R. The Dawning Era of Polymer Therapeutics. *Nat. Rev. Drug Discovery* **2003**, *2*, 347–360.
7. Haag, R.; Kratz, F. Polymer Therapeutics: Concepts and Applications. *Angew. Chem., Int. Ed.* **2006**, *45*, 1198–1215.
8. Immordino, M. L.; Dosio, F.; Cattel, L. Stealth Liposomes: Review of the Basic Science, Rationale, and Clinical Applications, Existing and Potential. *Int. J. Nanomed.* **2006**, *1*, 297–315.
9. Angelatos, A. S.; Katagiri, K.; Caruso, F. Bioinspired Colloidal Systems via Layer-by-Layer Assembly. *Soft Matter* **2006**, *2*, 18–23.
10. Schneider, G.; Decher, G. From Functional Core/Shell Nanoparticles Prepared Via Layer-by-Layer Deposition to Empty Nanospheres. *Nano Lett.* **2004**, *4*, 1833–1839.
11. Elbakry, A.; Zaky, A.; Liebl, R.; Rachel, R.; Goepferich, A.; Breunig, M. Layer-by-Layer Assembled Gold Nanoparticles for Sirna Delivery. *Nano Lett.* **2009**, *9*, 2059–2064.
12. Schneider, G. F.; Subr, V.; Ulbrich, K.; Decher, G. Multifunctional Cytotoxic Stealth Nanoparticles. A Model Approach with Potential for Cancer Therapy. *Nano Lett.* **2009**, *9*, 636–642.
13. Cortez, C.; Tomaskovic-Crook, E.; Johnston, A. P. R.; Radt, B.; Cody, S. H.; Scott, A. M.; Nice, E. C.; Heath, J. K.; Caruso, F. Targeting and Uptake of Multilayered Particles to Colorectal Cancer Cells. *Adv. Mater. (Weinheim, Ger.)* **2006**, *18*, 1998–2003.
14. De, K. S.; De, G. B. G.; Cuvelier, C.; Ferdinande, L.; Deckers, W.; Hennink, W. E.; De, S. S.; Mertens, N. In Vivo Cellular Uptake, Degradation, and Biocompatibility of Polyelectrolyte Microcapsules. *Adv. Funct. Mater.* **2007**, *17*, 3754–3763.
15. Sexton, A.; Whitney, P. G.; Chong, S.-F.; Zelikin, A. N.; Johnston, A. P. R.; De, R. R.; Brooks, A. G.; Caruso, F.; Kent, S. J. A Protective Vaccine Delivery System for in Vivo T Cell Stimulation Using Nanoengineered Polymer Hydrogel Capsules. *ACS Nano* **2009**, *3*, 3391–3400.
16. Saurer, E. M.; Jewell, C. M.; Kuchenreuther, J. M.; Lynn, D. M. Assembly of Erodible, DNA-Containing Thin Films on the Surfaces of Polymer Microparticles: Toward a Layer-by-Layer Approach to the Delivery of DNA to Antigen-Presenting Cells. *Acta Biomater.* **2009**, *5*, 913–924.
17. Ochs, C. J.; Such, G. K.; Caruso, F. Modular Assembly of Layer-by-Layer Capsules with Tailored Degradation Profiles. *Langmuir* **2010**, *27*, 1275–1280.
18. Chong, S.-F.; Lee, J. H.; Zelikin, A. N.; Caruso, F. Tuning the Permeability of Polymer Hydrogel Capsules: An Investigation of Cross-Linking Density, Membrane Thickness, and Cross-Linkers. *Langmuir* **2011**, *27*, 1724–1730.
19. Becker, A. L.; Johnston, A. P. R.; Caruso, F. Layer-by-Layer-Assembled Capsules and Films for Therapeutic Delivery. *Small* **2010**, *6*, 1836–1852.
20. Choi, C. H. J.; Alabi, C. A.; Websterb, P.; Davis, M. E. Mechanism of Active Targeting in Solid Tumors with Transferrin-Containing Gold Nanoparticles. *Proc. Natl. Acad. Sci. U. S. A.* **2010**, *107*), S1235/1–S1235/4.
21. Bartlett, D. W.; Su, H.; Hildebrandt, I. J.; Weber, W. A.; Davis, M. E. Impact of Tumor-Specific Targeting on the Biodistribution and Efficacy of Sirna Nanoparticles Measured by Multimodality in Vivo Imaging. *Proc. Natl. Acad. Sci. U. S. A.* **2007**, *104*, 15549–15554.
22. Kukowska-Latallo, J. F.; Candido, K. A.; Cao, Z.; Nigavekar, S. S.; Majoros, I. J.; Thomas, T. P.; Balogh, L. P.; Khan, M. K.; Baker, J. R., Jr. Nanoparticle Targeting of Anticancer Drug Improves Therapeutic Response in Animal Model of Human Epithelial Cancer. *Cancer Res.* **2005**, *65*, 5317–5324.
23. Kamphuis, M. M. J.; Johnston, A. P. R.; Such, G. K.; Dam, H. H.; Evans, R. A.; Scott, A. M.; Nice, E. C.; Heath, J. K.; Caruso, F. Targeting of Cancer Cells Using Click-Functionalized Polymer Capsules. *J. Am. Chem. Soc.* **2010**, *132*, 15881–15883.
24. Cortez, C.; Tomaskovic-Crook, E.; Johnston, A. P. R.; Scott, A. M.; Nice, E. C.; Heath, J. K.; Caruso, F. Influence of Size, Surface, Cell Line, and Kinetic Properties on the Specific Binding of A33 Antigen-Targeted Multilayered Particles and Capsules to Colorectal Cancer Cells. *ACS Nano* **2007**, *1*, 93–102.
25. Brown, J. M.; Wilson, W. R. Exploiting Tumor Hypoxia in Cancer Treatment. *Nat. Rev. Cancer* **2004**, *4*, 437–447.
26. Henning, T.; Kraus, M.; Brischwein, M.; Otto, A. M.; Wolf, B. Relevance of Tumor Microenvironment for Progression, Therapy and Drug Development. *Anti-Cancer Drugs* **2004**, *15*, 7–14.
27. Harris, T. J.; von, M. G.; Lord, M. E.; Park, J.-H.; Agrawal, A.; Min, D.-H.; Sailor, M. J.; Bhatia, S. N. Protease-Triggered Unveiling of Bioactive Nanoparticles. *Small* **2008**, *4*, 1307–1312.
28. Van, V. E.; Mincher, D.; Di, S. A.; Van, R. I.; Young, L.; Van, C. B.; Vanderkerken, K. Targeting an Mmp-9-Activated Prodrug to Multiple Myeloma-Diseased Bone Marrow: A Proof of Principle in the 5t33mm Mouse Model. *Leukemia* **2005**, *19*, 1628–1633.
29. Zalipsky, S.; Mullah, N.; Engbers, C.; Hutchins, M. U.; Kiwan, R. Thiolytically Cleavable Dithiobenzyl Urethane-Linked Polymer-Protein Conjugates as Macromolecular Prodrugs: Reversible Pegylation of Proteins. *Bioconjugate Chem.* **2007**, *18*, 1869–1878.
30. Lee, E. S.; Gao, Z.; Kim, D.; Park, K.; Kwon, I. C.; Bae, Y. H. Super pH-Sensitive Multifunctional Polymeric Micelle for Tumor Phe Specific Tat Exposure and Multidrug Resistance. *J. Controlled Release* **2008**, *129*, 228–236.
31. Lee, E. S.; Na, K.; Bae, Y. H. Super pH-Sensitive Multifunctional Polymeric Micelle. *Nano Lett.* **2005**, *5*, 325–329.
32. Wu, X. L.; Kim, J. H.; Koo, H.; Bae, S. M.; Shin, H.; Kim, M. S.; Lee, B.-H.; Park, R.-W.; Kim, I.-S.; Choi, K.; *et al*. Tumor-Targeting Peptide Conjugated pH-Responsive Micelles as a Potential Drug Carrier for Cancer Therapy. *Bioconjugate Chem.* **2010**, *21*, 208–213.
33. Koo, H.; Lee, H.; Lee, S.; Min, K. H.; Kim, M. S.; Lee, D. S.; Choi, Y.; Kwon, I. C.; Kim, K.; Jeong, S. Y. In Vivo Tumor Diagnosis and Photodynamic Therapy Via Tumoral pH-Responsive Polymeric Micelles. *Chem. Commun. (Cambridge, U. K.)* **2010**, *46*, 5668–5670.
34. Xu, J.; Tang, J.; Zhao, L.; Shen, Y. Advances in the Study of Tumor pH-Responsive Polymeric Micelles for Cancer Drug Targeting Delivery. *Yaoxue Xuebao* **2009**, *44*, 1328–1335.
35. Yang, X.; Grailer, J. J.; Pilla, S.; Steeber, D. A.; Gong, S.; Tumor-Targeting, pH-Responsive and Stable Unimolecular Micelles as Drug Nanocarriers for Targeted Cancer Therapy. *Bioconjugate Chem.* **2010**, *21*, 496–504.
36. Wu, X. L.; Kim, J. H.; Koo, H.; Bae, S. M.; Shin, H.; Kim, M. S.; Lee, B.-H.; Park, R.-W.; Kim, I.-S.; Choi, K.; *et al*. Tumor-Targeting Peptide Conjugated pH-Responsive Micelles as a Potential Drug Carrier for Cancer Therapy. *Bioconjugate Chem.* **2010**, *21*, 208–213.
37. Oishi, M.; Kataoka, K.; Nagasaki, Y. pH-Responsive Three-Layered Pegylated Polyplex Micelle Based on a Lactosylated Abc Triblock Copolymer as a Targetable and Endosome-Disruptive Nonviral Gene Vector. *Bioconjugate Chem.* **2006**, *17*, 677–688.
38. Gillies, E. R.; Fréchet, J. M. J. pH-Responsive Copolymer Assemblies for Controlled Release of Doxorubicin. *Bioconjugate Chem.* **2005**, *16*, 361–368.
39. Sullivan, R. M. *The Multifactorial Nature of Hypoxia-Induced Drug Resistance in Cancer: Involvement of Hypoxia-Inducible Factor 1*; 2008.
40. Tannock, I. F. Tumor Physiology and Drug Resistance. *Cancer Metastasis Rev.* **2001**, *20*, 123–132.
41. Michalski, B.; Banys, A.; Drosdzol, A.; Skrzypulec, V.; Mazurek, U. The Hypoxic Cell as a Target for Selective Cancer Therapy. *Przegl. Menopauzalny* **2009**, *8*, 196–201.
42. Jain, R. K. Normalizing Tumor Vasculature with Anti-Angiogenic Therapy: A New Paradigm for Combination Therapy. *Nat. Med. (N. Y., NY, U. S.)* **2001**, *7*, 987–989.
43. Inoue, H.; Sato, K.; Anzai, J. Disintegration of Layer-by-Layer Assemblies Composed of 2-Iminobiotin-Labeled

Poly(Ethyleneimine) and Avidin. *Biomacromolecules* **2005**, *6*, 27–29.
44. Lesch, H. P.; Kaikkonen, M. U.; Pikkarainen, J. T.; Yla-Herttuala, S., Avidin-Biotin Technology in Targeted Therapy. *Expert Opin. Drug Delivery 7*, 551-564.
45. Alexis, F.; Pridgen, E.; Molnar, L. K.; Farokhzad, O. C. Factors Affecting the Clearance and Biodistribution of Polymeric Nanoparticles. *Mol. Pharmaceutics* **2008**, *5*, 505–515.
46. Maeda, H.; Wu, J.; Sawa, T.; Matsumura, Y.; Hori, K. Tumor Vascular Permeability and the Epr Effect in Macromolecular Therapeutics. A Review. *J. Controlled Release* **2000**, *65*, 271–284.
47. Kjeken, R.; Mousavi, S. A.; Brech, A.; Griffiths, G.; Berg, T. Wortmannin-Sensitive Trafficking Steps in the Endocytic Pathway in Rat Liver Endothelial Cells. *Biochem. J.* **2001**, *357*, 497–503.
48. Kinsella, M. G.; Irvin, C.; Reidy, M. A.; Wight, T. N. Removal of Heparan Sulfate by Heparinase Treatment Inhibits Fgf-2-Dependent Smooth Muscle Cell Proliferation in Injured Rat Carotid Arteries. *Atherosclerosis (Amsterdam, Netherlands)* **2004**, *175*, 51–57.
49. Hansen, M.; Kilk, K.; Langel, U. Predicting Cell-Penetrating Peptides. *Adv. Drug Delivery Rev.* **2008**, *60*, 572–579.
50. Moghimi, S. M.; Hunter, A. C.; Murray, J. C. Long-Circulating and Target-Specific Nanoparticles: Theory to Practice. *Pharmacol. Rev.* **2001**, *53*, 283–318.
51. Pirollo, K. F.; Chang, E. H. Does a Targeting Ligand Influence Nanoparticle Tumor Localization or Uptake? *Trends Biotechnol.* **2008**, *26*, 552–558.
52. Greish, K. Enhanced Permeability and Retention (EPR) Effect for Anticancer Nanomedicine Drug Targeting. *Methods Mol. Biol. (Totowa, NJ, U. S.)* **2010**, *624*, 25−37.
53. Gittins, D. I.; Caruso, F. Tailoring the Polyelectrolyte Coating of Metal Nanoparticles. *J. Phys. Chem. B* **2001**, *105*, 6846–6852.